Ultrathin polarization-insensitive wide-angle broadband near-perfect absorber in the visible regime based on few-layer MoS_2 films

Yuebian Zhang, Wenwei Liu, Zhancheng Li, Hua Cheng, Yanbang Zhang, Guozhi Jia, Shuqi Chen, and Jianguo Tian

Citation: Appl. Phys. Lett. **111**, 111109 (2017); doi: 10.1063/1.4992045
View online: http://dx.doi.org/10.1063/1.4992045
View Table of Contents: http://aip.scitation.org/toc/apl/111/11
Published by the American Institute of Physics

Ultrathin polarization-insensitive wide-angle broadband near-perfect absorber in the visible regime based on few-layer MoS_2 films

Yuebian Zhang,[1] Wenwei Liu,[1] Zhancheng Li,[1] Hua Cheng,[1,a)] Yanbang Zhang,[2] Guozhi Jia,[2] Shuqi Chen,[1,a)] and Jianguo Tian[1]
[1]*The Key Laboratory of Weak Light Nonlinear Photonics, Ministry of Education, School of Physics and TEDA Institute of Applied Physics, Nankai University, Tianjin 300071, China*
[2]*School of Science, Tianjin Chengjian University, Tianjin 300384, China*

(Received 26 June 2017; accepted 4 September 2017; published online 15 September 2017)

We report the design, characterization, and experimental demonstration of a broadband near-perfect absorber in the visible regime based on strong interference in ultrathin molybdenum disulfide films obtained by the spin-coating method. The absorber is polarization-insensitive, and the absorption peak maintains a high value for large angles of incidence, which provides more efficient absorption for nonpolarized or oblique incident beams. The experimental results show that the absorption can reach more than 87% between 400 nm and 640 nm, which is in reasonable agreement with the simulated results. This work may offer a further step in the development of solar absorption-based nano-optoelectronic devices. *Published by AIP Publishing.*
[http://dx.doi.org/10.1063/1.4992045]

Optical absorbers play a key role in a variety of applications such as photodetectors,[1] microbolometers,[2] thermal imagers,[3] and solar energy conversion.[4,5] At optical frequencies, narrowband optical absorbers based on Fabry–Perot cavities[6,7] have been used for resonant cavity-enhanced photodetectors and similar devices. However, Fabry–Perot cavity-based absorbers are not very thin compared to the wavelength of light and are often narrowband or highly sensitive to the angle of incidence. Ultrathin absorbers utilizing the emerging concepts of metasurfaces have attracted much research attention.[8,9] As a result of different applications, the research interest in metamaterial absorbers has extended from single narrow bands to broadbands[10,11] and dual-bands or multibands.[12–14] Recently, the perfect absorber has also been extended to the bidirectional perfect absorber[15] and the integration of nearly perfect absorption and polarization conversion.[16] Unfortunately, these new absorber designs require patterning on subwavelength scales, which dramatically increases the fabrication costs and is therefore impractical for many large-scale optical and optoelectronic devices. Thus, there is a significant benefit to realizing ultrathin light-absorbing structures that require no micro- or nano-scale patterning.

Capasso *et al.* demonstrated that "ultrathin-film interference" effects can be observed by combining metals or metal-like materials with dielectrics featuring strong optical absorption.[17] The thickness of the films can be significantly reduced because of the nontrivial (not 0 or π) reflection phase shifts at the interfaces between one or more lossy materials. Recently, numerous material systems have been proposed to enhance the absorption based on this ultrathin film resonance concept, such as semiconductors on metallic substrates in the visible regime,[18–20] metal-dielectric composites on metals in the visible and near-infrared regimes,[21] and VO_2 on sapphire substrates in the mid-infrared regime.[22] However, it is difficult to reduce the thickness of covalently bonded, isotropic three-dimensional semiconductors to below 100 nm without significantly degrading the crystalline quality, increasing the defect density, or affecting the electronic charge transport by surface oxides and states.

On the other hand, there has been a large amount of research conducted on transition metal dichalcogenides (TMDs) in recent years because of their suitability for future electronic/optoelectronic device applications.[23–26] In particular, molybdenum disulfide (MoS_2), a semiconducting layered TMD, has been identified as one of the most promising two-dimensional (2D) materials for nano-electronic applications because its properties can be tuned by controlling the number of layers or carefully selecting substrate/gate dielectric materials.[27–29] However, the interaction between light and 2D materials is generally very small because of their very small thickness. It remains a great challenge to manipulate the flow of light using atomically thin MoS_2 and other 2D materials in the important visible and near-infrared spectral regions where they possess the most interesting optoelectronic properties.[30–33] To address the difficulties mentioned above, we can combine the two concepts of ultra-thin film resonance and TMDs. First, TMDs possess self-passivated, dangling bond- and oxide-free surfaces[34,35] and are thus attractive alternatives for ultra-thin absorbers when coupled with metals. Second, the interaction between light and thin 2D materials can increase dramatically by utilizing the unique geometry associated with ultrathin films.[36] In addition, the high refractive index and relatively high loss of MoS_2 in the visible spectral region make it particularly attractive for thin-film absorbers. Recently, Jariwala *et al.* demonstrated ultra-thin absorbers and Schottky junction devices using a micromechanically exfoliated WSe_2 structure on an Ag substrate.[37] Subsequently, they reported ultrathin van der Waals heterostructures exhibiting high photovoltaic quantum efficiency and high optical absorption based on exfoliated WSe_2/MoS_2

a)Authors to whom correspondence should be addressed: schen@nankai.edu.cn and hcheng@nankai.edu.cn

heterojunctions.[38] However, although mechanical exfoliation is a widely used method for preparing layered TMDs thin films, the difficulty in controlling the layer thickness and lateral size limitation, as well as the extremely low exfoliation yield, restricts the maximum realistic area of such devices. Recently, spin-coating methods, whereby dispersed solutions containing MoS_2 nanosheets are spin-coated on substrates, have been introduced.[39,40] This makes it possible to obtain large-area MoS_2 thin films with tunable thicknesses.

In this letter, we demonstrate a broadband near-perfect absorber in the visible regime based on strong interference in ultrathin MoS_2 films grown by the spin-coating method. A gold film is used as the metallic substrate because of its excellent stability in air. The simulated absorption can reach higher than 90% between 560 nm and 675 nm. The absorber is polarization-insensitive and robust to variations in the angle of incidence, which provides more efficient absorption for nonpolarized or oblique incident beams. The experimental results show that the absorption can reach more than 87% between 400 nm and 640 nm, which is in reasonable agreement with the simulated results. This study may provide a further step in the area of solar absorption by using layered material-based nano-optoelectronic devices.

A schematic of the ultra-thin perfect absorber is displayed in Fig. 1(a), in which a thin MoS_2 film of thickness h and complex refractive index $N_2 = n_2 + ik_2$ is sandwiched between air with refractive index $n_1 = 1$ and a semi-infinite metallic substrate with complex refractive index $N_3 = n_3 + ik_3$. Because of the high refractive index n_2 and high loss k_2 of the MoS_2 film in the visible spectral region, strong multiple reflections and nontrivial (not 0 or π) reflection phase shifts will occur at the interfaces when the light impinges on the structure [Fig. 1(b)]. The amplitude of the reflected light is the summation of the multiple reflections from the interfaces of the thin and high-index MoS_2 layer. In addition, the reflection and transmission coefficients for this structure can be analytically calculated with the following Fresnel–Airy formulas:[17]

$$r = \frac{r_{12} + r_{23}e^{2i\beta}}{1 + r_{12}r_{23}e^{2i\beta}}, \tag{1}$$

$$t = \frac{t_{12}t_{23}e^{i\beta}}{1 + r_{12}r_{23}e^{2i\beta}}, \tag{2}$$

where r_{ij} and t_{ij} are the polarization-dependent Fresnel coefficients and $\beta = 2\pi N_2 h\cos(\theta_2)/\lambda_0$, where λ_0 is the wavelength in a vacuum and θ_2 is the refraction angle in the MoS_2 layer. Then, the reflected power is $R = |r|^2$. For a MoS_2 film without an Au substrate, we can calculate the reflected power by assuming $N_3 = 1$. Moreover, in this situation, the power transmitted through the film can be written as $T = |t|^2$. As uniform films do not scatter light and energy must be conserved, the absorption in the film A_{film} is given by $A_{film} = 1 - R - T$. For a MoS_2 film on an Au substrate, because there is no transmission, the total absorption can be obtained as $A = 1 - R$. The perfect absorption condition, which corresponds to "zero-reflectance" when $T = 0$, can be obtained from the root of the numerator of Eq. (1), which corresponds to two equations that must be satisfied at the same time, an amplitude condition, and phase condition

$$|r_{21}| = |r_{23}|e^{-4\pi\frac{h}{\lambda_0}k_2} = |r_{23}|e^{-h\alpha_2}, \tag{3}$$

$$\phi_{23} + 2\phi_{prop} - \phi_{21} = 2\pi m, \tag{4}$$

respectively, where α_2 is the absorption coefficient of the thin film, $r_{ji} = -r_{ij}$, $r_{ij} = |r_{ij}|e^{i\phi_{ij}}$, ϕ_{ij} are the reflection phase shifts, ϕ_{prop} is the propagation phase pickup due to a single pass through the film, and m is an integer.

The optimized structure was achieved using the finite element method-based commercial software COMSOL Multiphysics. In the numerical simulations, the complex optical constants of bulk Au and MoS_2 films were taken

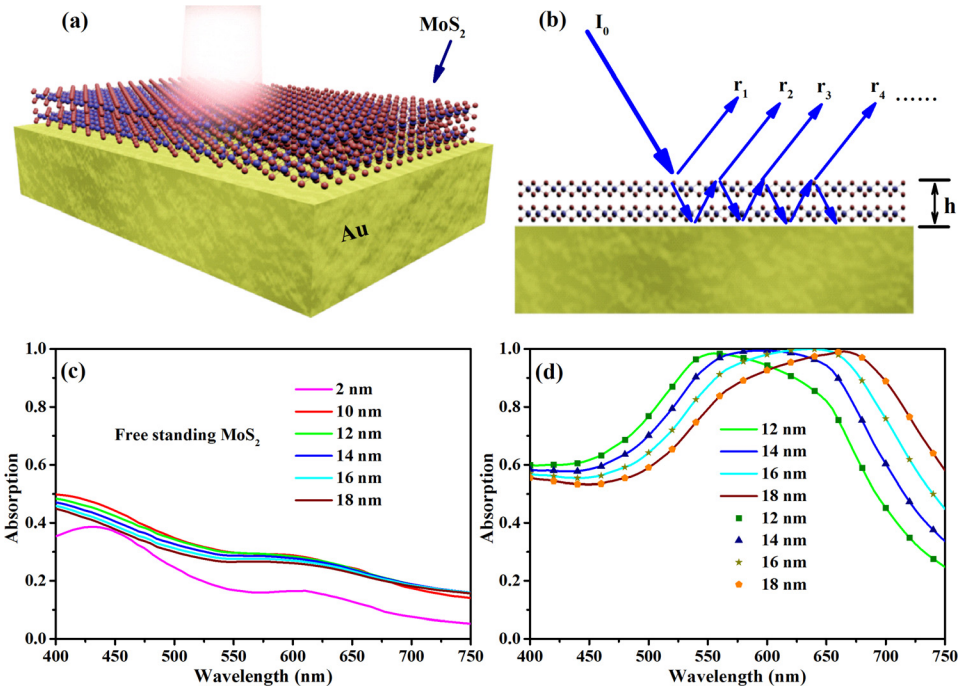

FIG. 1. (a) Schematic of the ultra-thin perfect absorber. The thickness of the MoS_2 layer is about 14 nm to 18 nm. (b) Schematic of the multiple reflections at the interfaces. (c) Simulated absorption in freestanding MoS_2 with various thicknesses. (d) Simulated (curves) and calculated (symbols) absorption spectra for various thicknesses of the MoS_2 film on the Au substrate.

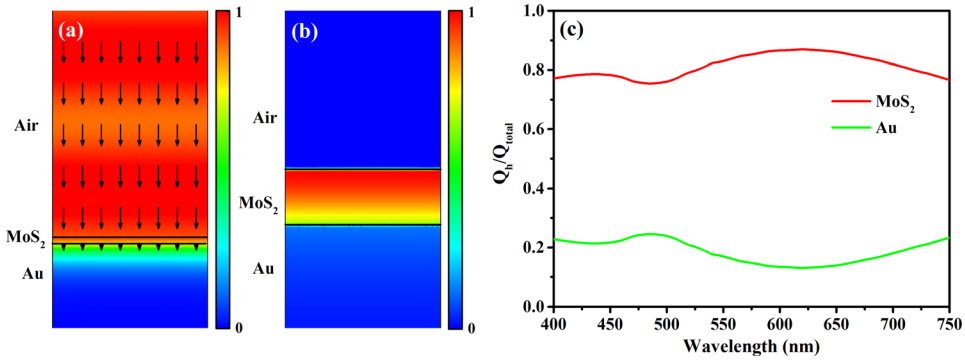

FIG. 2. (a) Simulated electric field amplitude distribution $|E|$ and time-averaged power flow $\vec{P}$ (arrows) at a wavelength of 600 nm. (b) Power dissipation density distribution Q_h under normal incidence at a wavelength of 600 nm. (c) Simulated power dissipation Q_h/Q_{total} in the MoS_2 layer and Au substrate. Q_{total} is the total absorbed power within the entire absorber.

from Refs. 41 and 42, respectively. The simulated absorption spectra for various thicknesses of the MoS_2 film in air and on the Au substrate are presented in Figs. 1(c) and 1(d), respectively. In Fig. 1(c), it can be seen that the total absorption is no more than 50% over the visible spectral region for all film thicknesses from 2 nm to 18 nm. However, the absorption can rise to nearly 100% for the MoS_2 film on the Au substrate in a specific wavelength range. This indicates that the coupling of the MoS_2 film with reflective metals is crucial for this resonantly enhanced absorption to occur. The optimal thickness of the MoS_2 film ranges from 14 nm to 18 nm, where the absorption peak can reach more than 99%. Furthermore, an absorption of more than 90% can be reached between 560 nm and 675 nm when the thickness of the MoS_2 film is 16 nm. The absorption peak undergoes a redshift with the increase in the MoS_2 thickness, suggesting a dependence on the optical path length. The absorption peak position can therefore be modulated by changing the thickness of the MoS_2 layer. We also calculated the absorption spectra for various thicknesses of the MoS_2 film on the Au substrate using the Fresnel–Airy formulas, and the results agree well with the simulated results.

To demonstrate the zero-reflectance condition of the absorber, we plot the electric field amplitude distribution $|E|$ under normal incidence at a wavelength of 600 nm with a MoS_2 film thickness of 14 nm [Fig. 2(a)]. It is observed that the electric field amplitude in the incident region almost maintains the same value, indicating that there is nearly no reflection from the absorber. Then, the absorption loss of the MoS_2 layer will induce perfect absorption of the incident light. This is illustrated by the time-averaged power flow $\vec{P}$ [arrows in Fig. 2(a)], which maintains the same optical intensity in the air but decays rapidly below the MoS_2 layer. To evaluate the absorption effects of the Au substrate, we plot the power dissipation density distribution q_h under normal incidence at a wavelength of 600 nm [Fig. 2(b)] and the normalized total power dissipation Q_h/Q_{total} in the MoS_2 layer and Au substrate for the 14 nm MoS_2 absorber [Fig. 2(c)]. Because all the materials considered are nonmagnetic, the power dissipation density (W/m^3) only contains resistive loss,[32] so $q_h = 1/2\epsilon_0\omega\epsilon_i|\vec{E}|^2$, where ϵ_0 is the vacuum permittivity, ω is the angular frequency, ϵ_i is the imaginary part of the dielectric function, and $\vec{E}$ is the electric field. The total power dissipation Q_h can be calculated by the volume integral of q_h within a volume V and then normalized to the total absorbed power within the entire absorber. As shown in Fig. 2(b), the heat generation density distribution Q_h is mostly located inside the MoS_2 layer rather than the Au substrate at the absorption peak. In addition, approximately 80% of the power is absorbed in the ultrathin MoS_2 film over the entire visible spectral region [Fig. 2(c)].

To demonstrate the performance of our designed absorber over a wide range of angles of incidence, we simulated the absorption spectra as functions of the wavelength and angle of incidence for both TE and TM polarizations, as shown in Figs. 3(a) and 3(b), respectively. We then calculated the absorption peak position at different angles of incidence using the multiple-wave interference theory, and the results agree well with our simulation. For the TE polarization, the absorption can still maintain a value as high as 91.9% at the angle of incidence of 50° at 610 nm. In addition, the absorption peak position does not change very much with the increase in the angle of incidence. This wide-angle property is mainly due to the small phase accumulation during the propagation through the ultrathin MoS_2 layer. For the TM polarization, the absorption can still maintain a value as high as 98.3% at the angle of incidence of 80° at 465 nm. However, when the angles of incidence change from 0° to

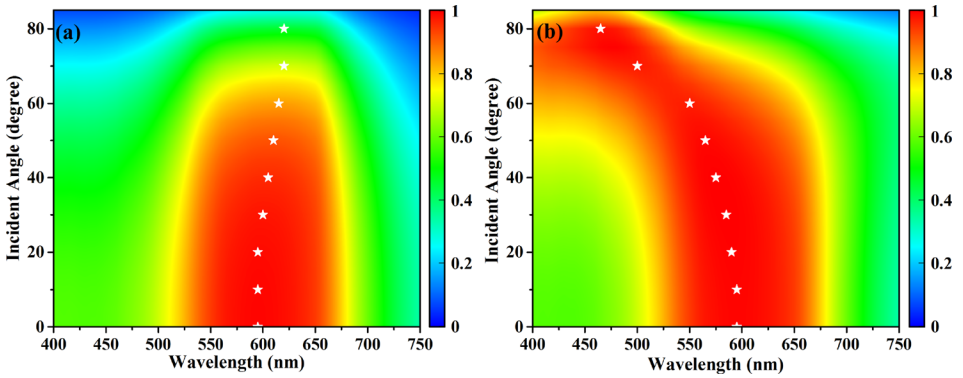

FIG. 3. Simulated absorption spectra of the 14-nm MoS_2 film absorber as functions of the wavelength and angle of incidence for (a) TE and (b) TM polarization. The calculated absorption peak positions are indicated by white star symbols at different angles of incidence.

80°, the absorption peak position for the TM polarization exhibits a blue-shift of 130 nm. This blue-shift phenomenon for the TM polarization is mainly due to the change in r_{12} with the increase in the angle of incidence. More specifically, for the TM polarization, with the change in the angle of incidence from 0° to 75°, $|r_{21}|$ will decrease and the reflection phase shift ϕ_{21} will increase. According to Eqs. (3)–(4), the zero-reflectance condition will be applied at shorter wavelengths, leading to a blue-shift of the absorption peak. These results reveal that the proposed ultrathin absorber operates quite well both for TE and TM radiation over a wide range of angles of incidence.

To demonstrate the absorber experimentally, a MoS_2 film was obtained by spin-coating the dispersed solution containing MoS_2 nanosheets on top of a glass substrate coated with 500-nm-thick gold by ion sputtering technology. To prepare the MoS_2-dispersed solution, we first dissolved MoS_2 powder in N-methyl-2-pyrrolidone (NMP) solution, purified it through ultrasonic treatment and centrifugation, and finally re-dispersed it into isopropyl alcohol solvent. To eliminate the impact of the residual NMP, we heated our sample in the annealing furnace at 300 °C. The results show that the residual NMP will affect slightly the absorption spectra. Figure 4(a) displays a scanning electron microscopy (SEM) image of the MoS_2 film, from which we know that the spin-coated film is composed of stacked MoS_2 nanosheets. Slightly overlapping crumpled sheets can be easily observed and are due to the agglomeration of the MoS_2 nanosheets in the drying process. Figure 4(b) displays the 3D atomic force microscopy (AFM) topology within a $30 \times 30\,\mu m^2$ area of the MoS_2 surface. From the AFM image, we know that the MoS_2 film is overall continuous but with a rough surface. The root mean square (RMS) roughness within the $30 \times 30\,\mu m^2$ area is approximately 27.7 nm. A homebuilt optical setup was used for the absorption measurement. Nonpolarized white light from a bromine tungsten lamp was focused on the sample with a 5×/0.13 microscope objective from the normal direction. The reflection spectrum was measured and then normalized to the reflection from an aluminum wafer in order to obtain the absolute reflection spectrum, $R(\lambda)$. In the absence of any transmission, the absorption spectrum can be obtained as $A(\lambda) = 1 - R(\lambda)$. The measured absorption spectrum of the MoS_2 film on the Au substrate is shown in Fig. 4(d). The experimental results show that an absorption higher than 90% can be reached between 400 nm and 700 nm, which covers most of the visible spectrum. Compared with the simulated result of the absorber with the 14 nm MoS_2 film in Fig. 1(d), the measured absorption spectra at short and long wavelengths slightly increase, leading to the broadening of the absorption spectrum. The complex refractive index of the MoS_2 film used in our simulation may have a small deviation from the actual value in our experiment. We measured the ellipsometric parameters of our MoS_2 film using spectroscopic ellipsometry. The complex refractive index and thickness of the MoS_2 film can be obtained. The extracted real (n) and imaginary (k) parts of the refractive index from ellipsometry measurements are shown in Fig. 4(c). The extracted film thickness is 10.3 nm. To estimate the scattering caused by the roughness of our sample, we simulated and measured the absorption spectra using different roughnesses of the sample and objectives with different numerical apertures in Fig. 4(d), respectively. We simulated the absorption spectrum of the absorber with roughness using the finite-difference time-domain approach based on the commercial software package, Lumerical Solutions. In our simulation, we imported the AFM data of our sample surface into the software and put it onto a 10.3 nm MoS_2 film. A $3.2 \times 3.2\,\mu m^2$ area was simulated, and all the scattered and reflected light was calculated. As shown in Fig. 4(d), the absorption peak reduces to 83% when taking the roughness into account, which is consistent with the experimental result. It should be noted that the RMS roughness of our Au substrate is 1 nm, which is far smaller than the wavelength of incident light and does not lead to far-field effects. When the numerical aperture of the objective changes from 0.13 to 0.55, the absorption peak undergoes a reduction from 97% to 90%. This is because the 5×/0.13 objective can only collect the specular reflection light, and the objective with larger numerical aperture can collect more

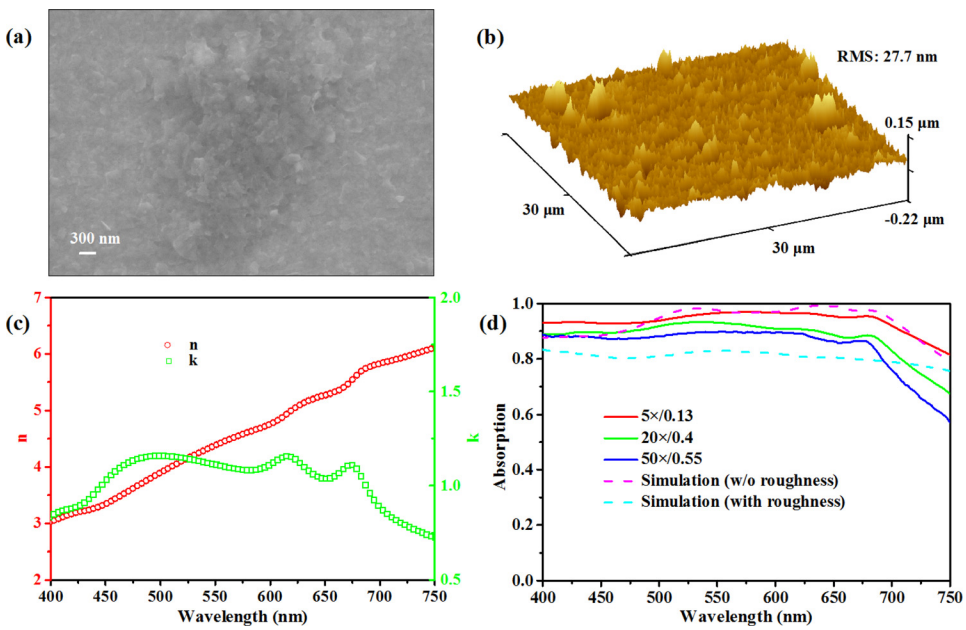

FIG. 4. (a) SEM image of the MoS_2 film. (b) AFM image of the sample surface. (c) Extracted real (n) and imaginary (k) parts of the refractive index of our MoS_2 film from ellipsometry measurements. (d) Simulated absorption spectra using the complex refractive index shown in (c) and measured absorption spectra of the MoS_2 absorber.

scattered light. However, the absorption can still remain higher than 87% between 400 nm and 640 nm when using the 50×/0.55 objective. Considering that the measured absorption spectra are the average effect of all thicknesses and all angles of incidence in our experiment, the small deviation between the experiment and simulation is in reasonable agreement.

In conclusion, an ultra-thin, broadband, near-perfect absorber made of MoS_2 films without structure patterning is demonstrated. The simulated absorption can reach more than 90% between 560 nm and 675 nm when the thickness of the MoS_2 film is 16 nm, with an absorption peak value of 99.98% at 635 nm. The absorber is polarization-insensitive, and the absorption peak maintains a high value at large angles of incidence for both TE and TM polarizations, which provides more efficient absorption for nonpolarized or oblique incident beams. The experimental results show that the absorption can reach more than 87% between 400 nm and 640 nm, which is in reasonable agreement with the simulated results. Our structure can be extended to other TMDs and other metal substrates, such as $WS_2/WSe_2/MoSe_2$ on Au/Ag/Cu substrates, and the absorption peak position can be modulated by changing the thickness of the TMD layer, making it more adaptable to potential applications. It is also worth noting that our ultra-thin near-perfect absorber requires no micro- or nano-scale patterning, and the TMD film can be grown by the spin-coating method, which makes it easier and inexpensive to produce in large areas. In addition, one can utilize the chemical vapor deposition and atomic layer deposition methods to further reduce the surface defects and height fluctuations of the MoS_2 film. In view of the potential applications of TMDs in electronic/optoelectronic devices, they may find numerous applications ranging from photodetectors and photovoltaic solar energy conversion to photoelectron-catalytic hydrogen evolution.

This work was supported by the National Key Research and Development Program of China (2016YFA0301102) and the Natural Science Foundation of China (Nos. 11574163, 61378006, and 11674240). We also acknowledge the support from the Collaborative Innovation Center of Extreme Optics, Shan xi University, Taiyuan, Shanxi 030006, China.

[1]O. Hayden, R. Agarwal, and C. M. Lieber, Nat. Mater. **5**, 352 (2006).
[2]P. L. Richards, J. Appl. Phys. **76**, 1 (1994).
[3]X. Liu, T. Starr, A. F. Starr, and W. J. Padilla, Phys. Rev. Lett. **104**, 207403 (2010).
[4]B. Tian, X. Zheng, T. J. Kempa, Y. Fang, N. Yu, G. Yu, J. Huang, and C. M. Lieber, Nature **449**, 885 (2007).
[5]S.-G. Yi, S. H. Kim, S. Park, D. Oh, H. Y. Choi, N. Lee, Y. J. Choi, and K.-H. Yoo, ACS Appl. Mater. Interfaces **8**, 33811 (2016).
[6]M. S. Ünlü and S. Strite, J. Appl. Phys. **78**, 607 (1995).
[7]R. M. Audet, E. H. Edwards, P. Wahl, and D. A. B. Miller, IEEE J. Quantum Electron. **48**, 198 (2012).
[8]Y. Ra'di, C. R. Simovski, and S. A. Tretyakov, Phys. Rev. Lett. **3**, 037001 (2015).
[9]N. Yu and F. Capasso, Nat. Mater. **13**, 139 (2014).
[10]J. Grant, Y. Ma, S. Saha, A. Khalid, and D. R. S. Cumming, Opt. Lett. **36**, 3476 (2011).
[11]S. Chen, H. Cheng, H. Yang, J. Li, X. Duan, C. Gu, and J. Tian, Appl. Phys. Lett. **99**, 253104 (2011).
[12]Q.-Y. Wen, H.-W. Zhang, Y.-S. Xie, Q.-H. Yang, and Y.-L. Liu, Appl. Phys. Lett. **95**, 241111 (2009).
[13]H. Cheng, S. Chen, H. Yang, J. Li, X. An, C. Gu, and J. Tian, J. Opt. **14**, 085102 (2012).
[14]D. Xiao, K. Tao, Q. Wang, Y. Ai, and Z. Ouyang, IEEE Photonics J. **9**, 1 (2017).
[15]J. Li, P. Yu, C. Tang, H. Cheng, J. Li, S. Chen, and J. Tian, Adv. Opt. Mater. **5**, 1700152 (2017).
[16]H. Cheng, X. Wei, P. Yu, Z. Li, Z. Liu, J. Li, S. Chen, and J. Tian, Appl. Phys. Lett. **110**, 171903 (2017).
[17]M. A. Kats and F. Capasso, Laser Photonics Rev. **10**, 699 (2016).
[18]M. A. Kats, R. Blanchard, P. Genevet, and F. Capasso, Nat. Mater. **12**, 20 (2012).
[19]J. Park, J.-H. Kang, A. P. Vasudev, D. T. Schoen, H. Kim, E. Hasman, and M. L. Brongersma, ACS Photonics **1**, 812 (2014).
[20]J. Park, S. J. Kim, and M. L. Brongersma, Opt. Lett. **40**, 1960 (2015).
[21]N. Zhang, K. Liu, H. Song, Z. Liu, D. Ji, X. Zeng, S. Jiang, and Q. Gan, Appl. Phys. Lett. **104**, 203112 (2014).
[22]M. A. Kats, D. Sharma, J. Lin, P. Genevet, R. Blanchard, Z. Yang, M. M. Qazilbash, D. N. Basov, S. Ramanathan, and F. Capasso, Appl. Phys. Lett. **101**, 221101 (2012).
[23]Q. H. Wang, K. Kalantar-Zadeh, A. Kis, J. N. Coleman, and M. S. Strano, Nat. Nanotechnol. **7**, 699 (2012).
[24]F. H. L. Koppens, D. E. Chang, and A. F. J. Garca, Nano Lett. **11**, 3370 (2011).
[25]Y. Choi, J. Kang, D. Jariwala, M. S. Kang, T. J. Marks, M. C. Hersam, and J. H. Cho, Adv. Mater. **28**, 3742 (2016).
[26]D. Jariwala, T. J. Marks, and M. C. Hersam, Nat. Mater. **16**, 170 (2017).
[27]A. B. Laursen, S. Kegns, S. Dahl, and I. Chorkendorff, Energy Environ. Sci. **5**, 5577 (2012).
[28]H. S. Lee, S.-W. Min, Y.-G. Chang, M. K. Park, T. Nam, H. Kim, J. H. Kim, S. Ryu, and S. Im, Nano Lett. **12**, 3695 (2012).
[29]B. Radisavljevic and A. Kis, Nat. Mater. **12**, 815 (2013).
[30]O. Lopez-Sanchez, D. Lembke, M. Kayci, A. Radenovic, and A. Kis, Nat. Nanotechnol. **8**, 497 (2013).
[31]L. Zhu, F. Liu, H. Lin, J. Hu, Z. Yu, X. Wang, and S. Fan, Light: Sci. Appl. **5**, e16052 (2016).
[32]B. Zhao, J. M. Zhao, and Z. M. Zhang, Appl. Phys. Lett. **105**, 031905 (2014).
[33]J. R. Piper and S. Fan, ACS Photonics **1**, 347 (2014).
[34]D. Jariwala, V. K. Sangwan, L. J. Lauhon, T. J. Marks, and M. C. Hersam, ACS Nano **8**, 1102 (2014).
[35]A. K. Geim and I. V. Grigorieva, Nature **499**, 419 (2013).
[36]J. Yang, Z. Wang, F. Wang, R. Xu, J. Tao, S. Zhang, Q. Qin, B. Luther-Davies, C. Jagadish, Z. Yu, and Y. Lu, Light: Sci. Appl. **5**, e16046 (2016).
[37]D. Jariwala, A. R. Davoyan, G. Tagliabue, M. C. Sherrott, J. Wong, and H. A. Atwater, Nano Lett. **16**, 5482 (2016).
[38]J. Wong, D. Jariwala, G. Tagliabue, K. Tat, A. R. Davoyan, M. C. Sherrott, and H. A. Atwater, ACS Nano **11**, 7230 (2017).
[39]J. N. Coleman, M. Lotya, A. ONeill, S. D. Bergin, P. J. King, U. Khan, K. Young, A. Gaucher, S. De, R. J. Smith, I. V. Shvets, S. K. Arora, G. Stanton, H.-Y. Kim, K. Lee, G. T. Kim, G. S. Duesberg, T. Hallam, J. J. Boland, J. J. Wang, J. F. Donegan, J. C. Grunlan, G. Moriarty, A. Shmeliov, R. J. Nicholls, J. M. Perkins, E. M. Grieveson, K. Theuwissen, D. W. McComb, P. D. Nellist, and V. Nicolosi, Science **331**, 568 (2011).
[40]Q. He, Z. Zeng, Z. Yin, H. Li, S. Wu, X. Huang, and H. Zhang, Small **8**, 2994 (2012).
[41]E. D. Palik, *Handbook of Optical Constants of Solids* (Academic, Orlando, FL, 1985), Vol. I.
[42]D. Li, X. Song, J. Xu, Z. Wang, R. Zhang, P. Zhou, H. Zhang, R. Huang, S. Wang, Y. Zheng, D. Zhang, and L. Chen, Appl. Surf. Sci. **421**, 884 (2017).